Supporting Material for

Hyperbolic Tiling on the Gyroid Membrane in ABC Star Block Copolymers

Kenichi Hayashida, Tomonari Dotera*, Junichi Matsuzawa,

Atsushi Takano, Yushu Matsushita

This PDF file includes:

Materials and Methods

tables S1, S2

Figs. S1, S2, S3, S4, S5, S6

Contents

table S I: Characteristics of the ISP Star-Shaped Block Copolymer Samples

Sample	$M_n \times 10^{-3}$	Mw/Mn^a	Formulation (weight fraction)	$\Phi_I : \Phi_S : \Phi_P{}^b$
I precursor	13.3^c	1.04	-	-
S precursor	27.4^a	1.01	-	-
I_1-b-$S_{1.8}$	40.7^d	1.03	-	1.00 : 1.82 : 0.00
$I_1S_{1.8}P_{3.2}$	92.1^d	1.02	-	1.00 : 1.83 : 3.17
$I_1S_{1.8}P_{3.5}$	-	-	$I_1S_{1.8}P_{3.2}/I_1S_{1.8}P_{4.3}$ (0.657/0.343)	1.00 : 1.83 : 3.49
$I_1S_{1.8}P_{3.8}$	-	-	$I_1S_{1.8}P_{3.2}/I_1S_{1.8}P_{4.3}$ (0.329/0.671)	1.00 : 1.83 : 3.84
$I_1S_{1.8}P_{4.0}$	-	-	$I_1S_{1.8}P_{3.2}/I_1S_{1.8}P_{4.3}$ (0.200/0.800)	1.00 : 1.83 : 3.99
$I_1S_{1.8}P_{4.3}$	110^d	1.01	-	1.00 : 1.83 : 4.25

[a]Determined by SEC using polystyrene standard samples.

[b]Volume ratios of I:S:P were calculated using bulk densities of the components, i.e., 0.926, 1.05, and 1.14 g/cm^3 for the I, S, and P components, respectively.

[c]Determined by ^{1}H NMR.

[d]Estimated by ^{1}H NMR based on M_n of the S precursor.

I. MATERIALS AND METHODS

Sample Preparation: ABC Star-shaped block copolymer samples composed of polyisoprene (I), polystyrene (S) and poly(2-vinylpyridine) (P) were synthesized by anionic polymerizations as reported previously.[1] Table SI summarizes the volume ratios of the three components in two ISP star-shaped block polymer samples used in this study together with their molecular weights and molecular weight distributions (MWDs). Three other samples were also obtained by blending the two star polymers as shown in table SI. Their compositions were determined using a 500 MHz ^{1}H NMR spectrometer (Varian Inc., Unity Inova 500). The number-average molecular weight of the common S precursor and the MWDs of the entire polymer samples were determined by SEC calibrated with standard polystyrene samples. These analyses were carried out using an SEC system (Tosoh Ltd.) equipped with a set of three separation columns of 300 mm × 7.8mm i.d. -G4000$_{HR}$ and a refractive index detector (RI-8021).

[1] A. Takano, *et al.*, *Macromolecules* **37**, 9941-9946 (2004).

table S II: Morphological Transition for the $I_1S_{1.8}P_X$ Star-Shaped Block Copolymers

X	morphology	combined I and S domain	P domain	Φ_P [a]
0	cylinder	-	-	0.00
0.8-2.9	tiling-cylinders[b]	matrix	cylinder	0.22-0.51
3.2-3.8	hyperbolic tiling-on-gyroid	membrane	network	0.53-0.58
4.0-11	cylinders-in-lamella	lamella	lamella	0.59-0.80
12-32	lamellae-in-cylinder	cylinder	matrix	0.81-0.92
53	lamellae-in-sphere	sphere	matrix	0.95

[a]Volume fraction of the P component.

[b]Identified in the previous work for the same $I_1S_{1.8}P_X$ series.

Morphological Observations: Sample films were obtained by solvent-casting from 5% solutions of the ISP star polymer samples in THF for 2 days. The films were dried at room temperature for 12 h and annealed at 170 °C under a vacuum for 3 days.

For TEM observations, the films were cut into ultrathin sections having a thickness of 50 or 100 nm using an ultramicrotome (Reica Ultracut FCS), and they were observed on a transmission electron microscope (Hitachi, H-800).

Microbeam SAXS measurements were performed using beamline BL40XU at SPring-8 facility (Hyogo, Japan). The wavelength of the X-ray was 0.12 nm, and the size of the X-ray microbeam was approximately 5 μm $\times$ 5 μm (fwhm). The precise camera length was calibrated using a standard collagen sample. For the microbeam SAXS measurements, the annealed sample films were cut into thin sections with a thickness of 30 μm using an ultramicrotome (Reica, Ultracut FCS) with a diamond knife (Diatome, cryo T). These polymer samples were placed on a sample stage and scanned in 1-10 μm steps to look for the crystal planes of the sample parallel to the incident beam.

II. PHASE BEHAVIOUR OF THE ISP STAR-SHAPED BLOCK COPOLYMER

Table SII summarizes the morphologies formed by the $I_1S_{1.8}P_X$ star-shaped block copolymers which have been identified in our consecutive works. The shapes of the combined domains made of the I and S components are varied from matrix to membranes, to lamel-

lae, to cylinders, and to spheres, while those of the P domains are varied from cylinders to networks, to lamellae, and to matrix with increasing X. This morphological transition is analogous to that of AB-diblock copolymers.

One might imagine that the inverse network structure consisting of the I plus S domains divided by a gyroid membrane composed of the P component may exist in the composition range between cylinders-in-lamella (Fig. 1(c)) and lamellae-in-cylinder (Fig. 1(b)). However, we could not find the structure in spite of thorough TEM observations in this region ($11 \leq X \leq 12$).

III. ESCHER'S CIRCLE LIMIT IV

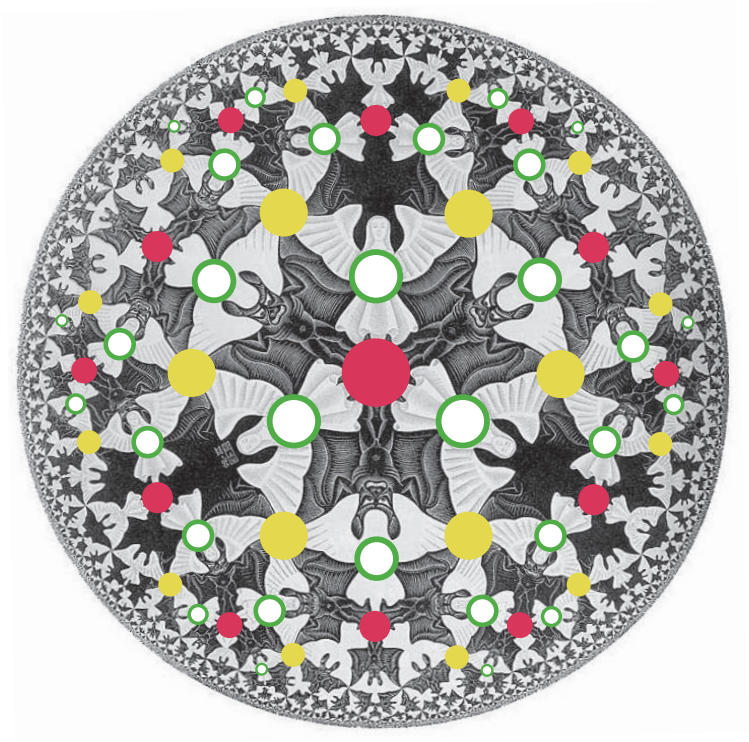

Fig.S 1: Circle Limit IV (Heaven and Hell) superimposed by the hyperbolic Archimedean tiling (3^3.4.3.4) vertices (green circles).

IV. SADDLE POINTS OF THE GYROID SURFACE

Site symmetry points, .$\bar{3}$. and $\bar{4}$.. of space group $Ia\bar{3}d$, are denoted as 16a and 24d, representing multiplicity and Wyckoff letter. Sixteen positions of 16a are located at (0,0,0), (1/2,0,1/2), (0,1/2,1/2), (1/2,1/2,0), (3/4,1/4,1/4), (3/4,3/4,3/4), (1/4,1/4,3/4), (1/4,3/4,1/4), and translated ones with (1/2,1/2,1/2). They constitute a BCC lattice with a half lattice constant, and are monkey saddle points as shown in Fig.S2A.

Twenty-four positions of 24d are (3/8,0,1/4), (1/8,0,3/4), (1/4,3/8,0), (3/4,1/8,0), (0,1/4,3/8), (0,3/4,1/8), (3/4,5/8,0), (3/4,3/8,1/2), (1/8,1/2,1/4), (7/8,0,1/4), (0,1/4,7/8), (1/2,1/4,1/8), and translated ones with (1/2,1/2,1/2). They are (horse) saddle points of the surface. See Fig.S2B.

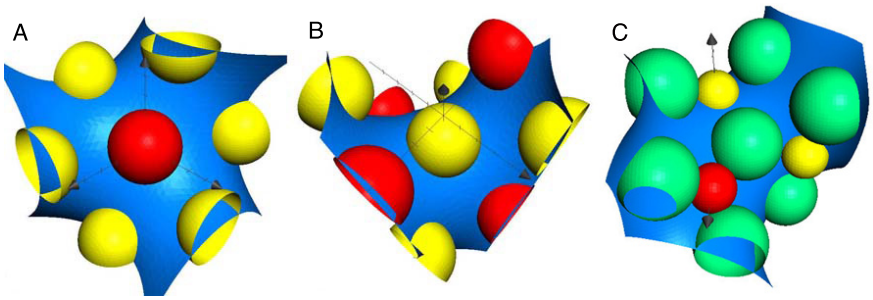

Fig.S 2: (**A**) 16a (red) and (**B**) 24d (yellow) positions. G surface is depicted in blue. They are monkey saddle and horse saddle points, respectively. (**C**) Vertices (green) of the (3^3.4.3.4) tiling.

V. WEIERSTRASS AND ENNEPER REPRESENTATION

According to Ref.8,[2] the gyroid minimal surface is evaluated by the Weierstrass and Enneper representation:

$$(x,y,z) \;=\; \mathrm{Re}\left(e^{i\alpha}\int_0^{\omega}(1-\omega'^2)R(\omega')\mathrm{d}\omega', e^{i\alpha}\int_0^{\omega} i(1+\omega'^2)R(\omega')\mathrm{d}\omega', e^{i\alpha}\int_0^{\omega} 2\omega'^2 R(\omega')\mathrm{d}\omega'\right),$$

where $R(\omega)$ is given by

$$R(\omega) = \frac{1}{\sqrt{1-14\omega^4+\omega^8}}$$

[2] A. H. Schoen, "Infinite periodic minimal surfaces without self-intersections" (NASA Technical Note, TN D-5541, 1970).

for the P, D, and G triply periodic minimal surfaces. The Bonnet angle for the G surface is exactly written as

$$\alpha = \cot^{-1}\left[\frac{K(\sqrt{3}/2)}{K(1/2)}\right] \fallingdotseq 38.0147^\circ,$$

where $K(x)$ is the complete elliptic integral of the first kind. We calculated these integrals using the incomplete elliptic integrals of the first kind for the shaded region in the complex plane (Fig.S3). We indicate red, yellow and green points, which are mapped to saddle points $16a$ and $24d$, and to a vertex of the $(3^3.4.3.4)$ tiling on the G surfece, respectively. Applying suitable scaling, rotation and displacement transformations, we could find the coordinates of vertices given in the paper. Note that the values are the same as those obtained by the approximation form

$$\sin 2\pi x \cos 2\pi y + \sin 2\pi y \cos 2\pi z + \sin 2\pi z \cos 2\pi x = 0,$$

up to three digits. The full surface can be easily generated by the symmetry operation of the space group $I\bar{4}3d$. Detailed mathematical arguments will be published elsewhere[3].

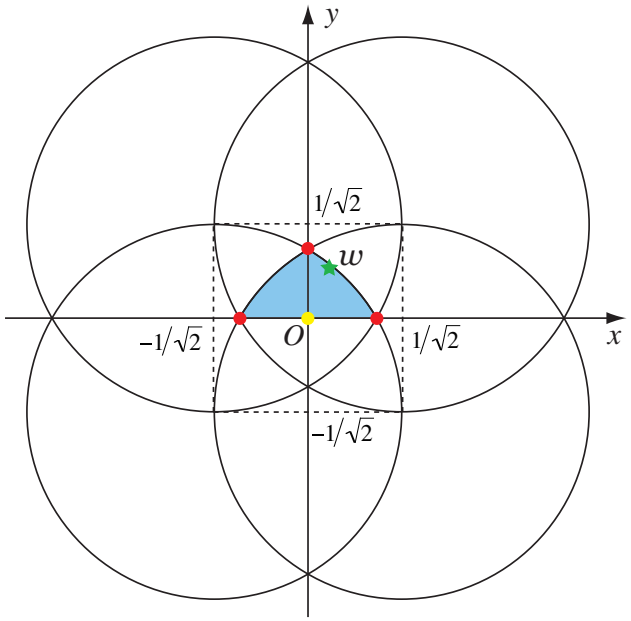

Fig.S 3: The region of ω for the integrals of the Weierstrass and Enneper representation. The blue region is minimal for the space group $I\bar{4}3d$. Red and yellow circles are mapped to $16a$ and $24d$ saddle points, respectively. The green star is mapped to a vertex of the $(3^3.4.3.4)$ tiling.

[3] T. Dotera and J. Matsuzawa, to be published in Kokyuroku, RIMS, Kyoto University.

VI. ADDITIONAL RESULTS OF TEM OBSERVATION

A. TEM stained with I_2

We show an image of the [001] projection for the $I_{1.0}S_{1.8}P_{3.2}$ sample demonstrating an interesting symmetry by chance, which provides an additional evidence of the space group. See Fig.S4A. There are left-hand and right-hand windmills located at the centers of squares and the pattern show the plane group $p4gm$. We point out that the centers of squares correspond to 4_1 and 4_3 screw axes of the space group $Ia\bar{3}d$. The lattice constant a is estimated from the relationship; $a = (\sqrt{2} + \sqrt{6})d'/2$, where d' denotes the edge-length of squares. The average value of d' in Fig.S4 gives a lattice constant of ∼90 nm, which agrees with other estimations. TEM simulation perpendicular to the [001] direction is shown in Fig.S4B. The relative contrast was represented by 0.3 for S and I, 1.0 for P in the case of I_2. When the sample is thin enough, say, $0.5a$, and the place is fine-tuned, the simulation reproduces the tiling structure.

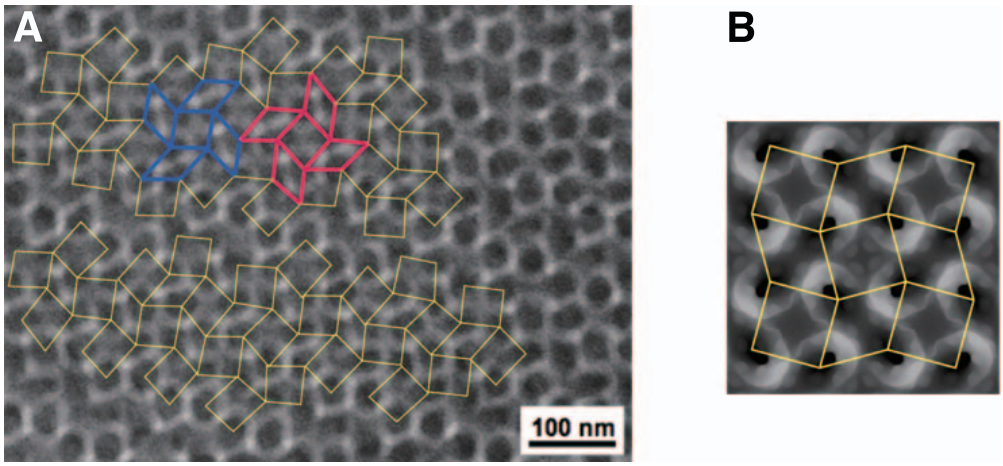

Fig.S 4: (**A**) TEM image of the [001] projection for the $I_{1.0}S_{1.8}P_{3.2}$ sample stained with I_2. Two domains of tiling structures with $p4gm$ plane group are superimposed. The center of a square corresponds to the 4_1 or 4_3 screw axis of $Ia\bar{3}d$. (**B**) TEM simulation stained with I_2, perpendicular to [001] for the (3^3.4.3.4) model. The thickness is $0.5a$, and the z-coordinate is from $0.125a$ to $0.625a$, where a is the lattice constant.

B. TEM stained with OsO_4

The osmium tetroxide (OsO_4) stains the I component heavily, thus the shape of I domains are investigated. We find following facts which are the basis of the model structure:
(1) The I component constitute isolated domains as shown in Fig.S5. To check the domains are compact, we show a series of TEM images of the $I_1S_{1.8}P_{3.2}$ sample at the same sample location with different tilt angles. TEM images were taken with a tilt angle range of $-20° \leq \phi \leq 20°$ in 10° steps obtained by inclining the sample stage on a horizontal axis, where the sample was cut into ultrathin sections of 50 nm thickness and stained with OsO_4. As the sample is tilted from -20° to 20°, the black I phase appears to form isolated domains, not to form infinite cylinders, nor networks.
(2) The isolated I domains look prolate (rodlike), but not oblate (disklike).
(3) The distance between ellipsoids appears to be equal to or greater than 25 nm.
(4) Local square arrangement is observed.

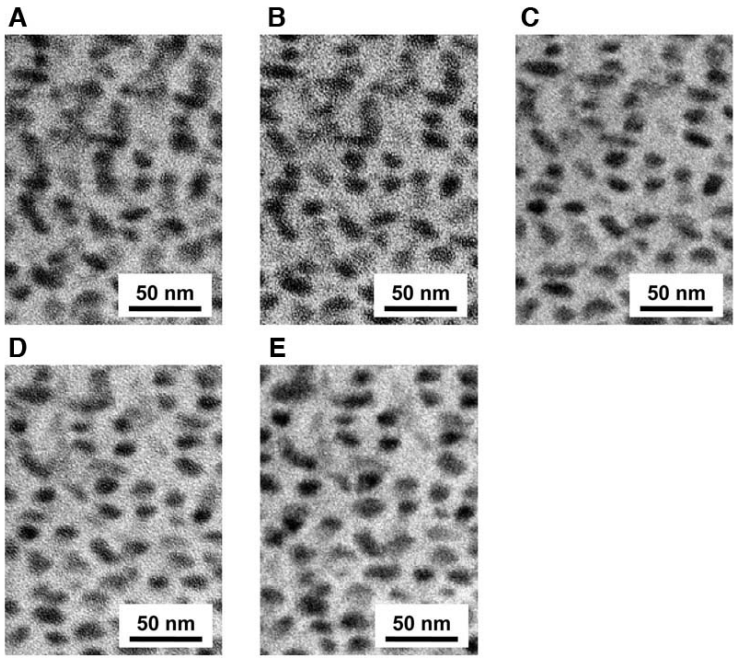

Fig.S 5: TEM images of the $I_1S_{1.8}P_{3.2}$ sample taken with tilt angles of (**A**) -20 °, (**B**) -10°, (**C**) 0°, (**D**) 10°, and (**E**) 20° by inclining the sample around a horizontal axis. The sample was cut into ultrathin sections of about 50 nm thickness and stained with OsO_4.

VII. SIMULATION OF X-RAY SCATTERING

The scattering potential, which is proportional to electron densities for each component, is given by $f(\boldsymbol{r}) = 3.12$, 3.40, and 3.66, for I, S, and P, respectively. The scattering intensity is proportional to $|f_{\rm t}(\boldsymbol{q})|^2$, where $f_{\rm t}(\boldsymbol{q})$ is the Fourier transform of $f(\boldsymbol{r})$. To quantify, we calculate spherically averaged intensities as a function of $q = (2\pi/a)\sqrt{h^2+k^2+l^2}$, where h, k, and l are scattering indexes, and where a is the lattice constant. See Fig.S6. Common logarithms $\log I$ as a function of q is plotted, where I is the spherically averaged intensity of I_{hkl} divided by I_{000}. We find followings:

(1) $\sqrt{6}$ ($\{211\}$) and $\sqrt{8}$ ($\{220\}$) are strong as expected for the gyroid structure.

(2) $\sqrt{16}$ ($\{400\}$) is stronger than $\sqrt{20}$ ($\{420\}$). The SAXS experiment shows in Fig.3A that $\{400\}$ is stronger.

(3) $\sqrt{22}$ ($\{332\}$) is the third strongest. The SAXS experiment shows in Fig.3B that it is the third strongest.

(4) $\sqrt{26}$ ($\{431\}$) is seen. The SAXS experiment shows in Fig.3C that it is visible.

(5) $\sqrt{10}$ is seen for (3^3.4.3.4), whose $\{310\}$ peak is disallowed for $Ia\bar{3}d$, but permitted for $I\bar{4}3d$.[4] However, the calculated value is too small to be detected in SAX experiments.

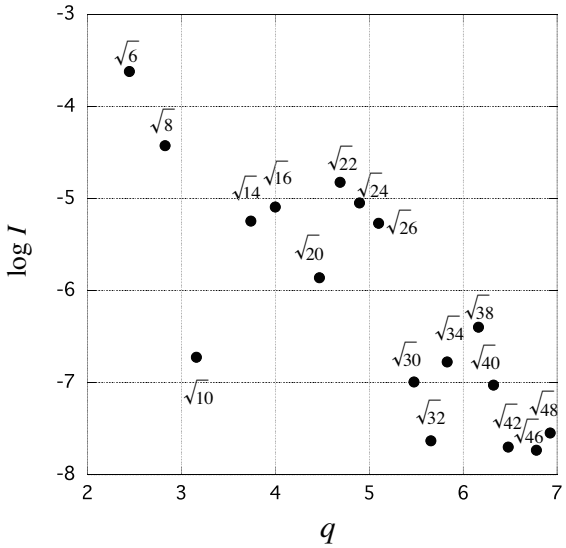

Fig.S 6: Plot of calculated intensity for the model (3^3.4.3.4).

[4] The reflection conditions of $I\bar{4}3d$ are almost the same as those of $Ia\bar{3}d$ except $0kl$ type: $k+l = 2n$ ($I\bar{4}3d$) or $k, l = 2n$ ($Ia\bar{3}d$). Thus we may detect $\{310\}$ peaks for (3^3.4.3.4) with $I\bar{4}3d$.